Available online at www.sciencedirect.com
SCIENCE DIRECT
Trans. Nonferrous Met. Soc. China 16(2006) 274−280
Transactions of Nonferrous Metals Society of China
www.csu.edu.cn/ysxb/

Deformation behavior and mechanisms of Ti-1023 alloy

BAO Ru-qiang(鲍如强), HUANG Xu(黄 旭), CAO Chun-xiao(曹春晓)
Beijing Institute of Aeronautical Materials, Beijing 100095, China

Received 15 June 2005; accepted 15 November 2005

Abstract: The deformation behavior and mechanisms of Ti-1023 alloy were studied in the temperature range of 650−900 ℃ and strain rate range of 0.001−10 s^{-1} by compression and tensile tests. The results show that in a limited strain rate range of 0.001−0.1 s^{-1}, the kinetic rate equation is obeyed and a linear fit is obtained at all the temperatures. The apparent activation energy is 322 kJ/mol in the α-β region and 160 kJ/mol in the β region, respectively. Power dissipation maps of this alloy developed by using Gleeble test data show three domains in the tested range. Superplasticity, marked by abnormal elongation at 700 ℃, occurs in the temperature range of 650−750 ℃ and at strain rates below about 0.03 s^{-1}. Large grain superplasticity takes place in the temperature range of 750−850 ℃ and strain rates range of 0.001−0.03 s^{-1}. Dynamic recrystallization occurs in the temperature range of 850-900 ℃ and at strain rates below about 1 s^{-1}. The instability maps of this alloy were also developed.

Key words: Ti-1023 alloy; deformation behavior; deformation mechanisms; processing maps; superplasticity

1 Introduction

Beta titanium alloys offer a variety of microstructural morphologies and associated mechanical property variations thus giving considerable latitude in microstructure design. They are the most versatile class of titanium alloys and offer the highest strength to mass ratios and deepest hardenability among titanium alloys[1]. They also possess excellent hot workability and very attractive combinations of strength, toughness and fatigue resistance at large cross sections[2,3]. The metastableTi-1023 alloy may be forged at relatively low temperatures and heat treated to achieve strengths as high as 1 200−1 400 MPa, with elongation in the range 4%−10%. While the microstructure-property correlations in this alloy have been established by several investigators[4−6], limited information is available on the mechanisms of hot deformation[7]. The objective of this study is to model the microstructural mechanisms of hot deformation of Ti-1023 alloy in a wide range of temperature and strain rate so that windows for industrial processing may be identified for optimizing workability and controlling microstructure.

Several approaches of modelings are employed to evaluate the mechanisms and hot deformation behavior of metallic materials, including analysis of shapes of stress—strain curves, kinetic analysis and processing maps[8,9]. Especially in recent years, processing maps are being used to design hot working schedules for making near-net shapes in a wide variety of materials. Developed on the basis of dynamic materials modeling, processing maps not only present the domains in which a decisive deformation mechanism of specific microstructure takes place, but also describe the instability regimes which should be avoided during hot working[10]. Furthermore, optimal hot workability temperature and strain rate are available through processing maps[11]. And thus, processing maps provide a strong method to optimize and design the hot processes of materials and more effectively obtain desirable microstructure or control microstructure by hot processes. To better understand the deformation behavior of Ti-1023 alloy, the mechanisms of this alloy were studied by using processing maps and other materials models.

2 Experimental

2.1 Materials

The detailed chemical composition(mass fraction, %) of Ti-1023 alloy used in this paper is 10.2 V, 1.8 Fe, 3.1 Al, 0.11 O, 0.01 N, 0.02 C, ≤0.001 H, and balance Ti. The β transus was determined to be (802±3) ℃ and the microstructure of as-received material shown in Fig.1

Corresponding author: BAO Ru-qiang; Tel: +86-10-62496633; E-mail: ruqiang.bao@biam.ac.cn

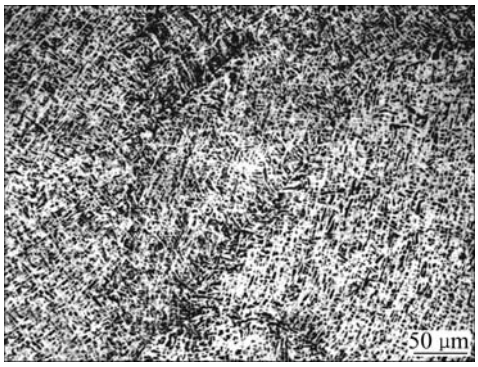

Fig.1 Optical microstructure of as-received material

is composed of β phase and elongated α phase.

2.2 Compression testing

Compression specimens of 12 mm in height and 8 mm in diameter were machined for testing under all conditions. A thermocouple welded at mid span of the specimens was used to control and measure the actual temperature of the specimens. Graphite pieces were plastered for lubrication on two ends of the specimen. The tests were carried out on the Gleeble3500 thermal stimulation machine in temperature range 650−900 ℃ at an interval of 50 ℃ and true strain rates of 0.001, 0.01, 0.1, 1, and 10 s^{-1}. The specimens were heated to applied temperature in 1 min and held at the applied temperature for 2 min before deformation. The specimens were deformed to impose a true strain of about 0.6 and were air-cooled to room temperature after deformation. Deformed specimens were sectioned parallel to the compression axis and the cut surface was prepared for metallographic examination. The specimens were etched by 30 mL H_2O_2(30%)+5 drops HF solution. Metallographs were observed on NEOPHOT-21 optical microscopy and TEM was carried out on JEM-2000FX.

2.3 Tensile testing

Tensile tests were conducted in the temperature range of 650−900 ℃ at a nominal strain rate of 0.001 s^{-1} (constant actuator speed of 1.1 mm/min) in the testing apparatus of superplasticity. Cylindrical specimens of 25 mm in gauge length and 5 mm in diameter were used for this purpose. The specimens were pulled to fracture and total elongation as a function of temperature was recorded.

3 Results and discussion

3.1 Stress—strain behavior

The shapes of stress—strain curves indicate some features that help identify the mechanisms of hot deformation, although not in a conclusive fashion. Curves with typical features are given in Fig.2. From which some features can be seen as follows.

1) At strain rate slower than 0.1 s^{-1} (Figs.2(a), (c) and (d)), the curves show the phenomena of work hardening, indicating that the mechanisms may be dynamic recrystallization, superplasticity, globularization of acicular α or dynamic recovery. And the change of true stress of the alloy deformed in the α-β field with the temperature and strain rate is greater than that deformed above β transus. This shows that the effect of α phase with hcp structure on true stress is significantly greater than β phase having bcc structure.

2) At strain rate higher than 0.1 s^{-1} in the α-β field(＞700 ℃) as shown in Figs.2(b) and (c), the curves exhibit flow softening after a critical strain leading to a steady state, indicating that the mechanisms of softening are sufficiently fast to exceed or balance the rate of work hardening. But in β field the work hardening curves are still obtained. All curves indicate that the possible mechanisms are dynamic recrystallization, and globularization of acicular α.

3) At higher strain rates (＞0.1 s^{-1}) in the α-β field (＜700 ℃), the material exhibits a continuous flow softening behavior. Such a feature is observed for globularization process of acicular structures, flow instability due to flow localization, or micro-cracking during deformation[9,10]. Detailed microstructural examination is required to decide them.

4) Ti-1023 alloy has lower flow stress than any other titanium alloy, and so it is more suitable for isothermal forging or hot die forging with lower manufacture cost due to lower forging temperature and cheaper die. At lower strain rate (＜0.1 s^{-1}), this alloy deformed in the α-β field has higher peak stress(Fig.3(a)) and steady stress(Fig.3(b)) than that deformed in β field, especially for temperature lower than 750℃. If forging is conducted at temperature lower than 750 ℃, the larger capacity of press is required.

3.2 Kinetic analysis

The steady state flow stress in hot deformation is related to strain rate and temperature through an Arrhenius type of rate equation

$$\dot{\varepsilon} = A\sigma^n \exp(-Q/RT) \quad (1)$$

where $\dot{\varepsilon}$ is strain rate; σ is flow stress; A is frequency factor; Q is apparent activation energy; R is gas constant; T is temperature in Kelvin, and n is stress exponent. In order to identify the mechanism(s) of hot deformation, the kinetic parameters, n and Q in Eqn.(1), are to be evaluated. The variation of flow stress with strain rate is shown in Fig.4. The inverse of the slope of this curve represents the stress exponent, n. This plot is excepted to show a linear relationship if Eqn.(1) is valid. However,

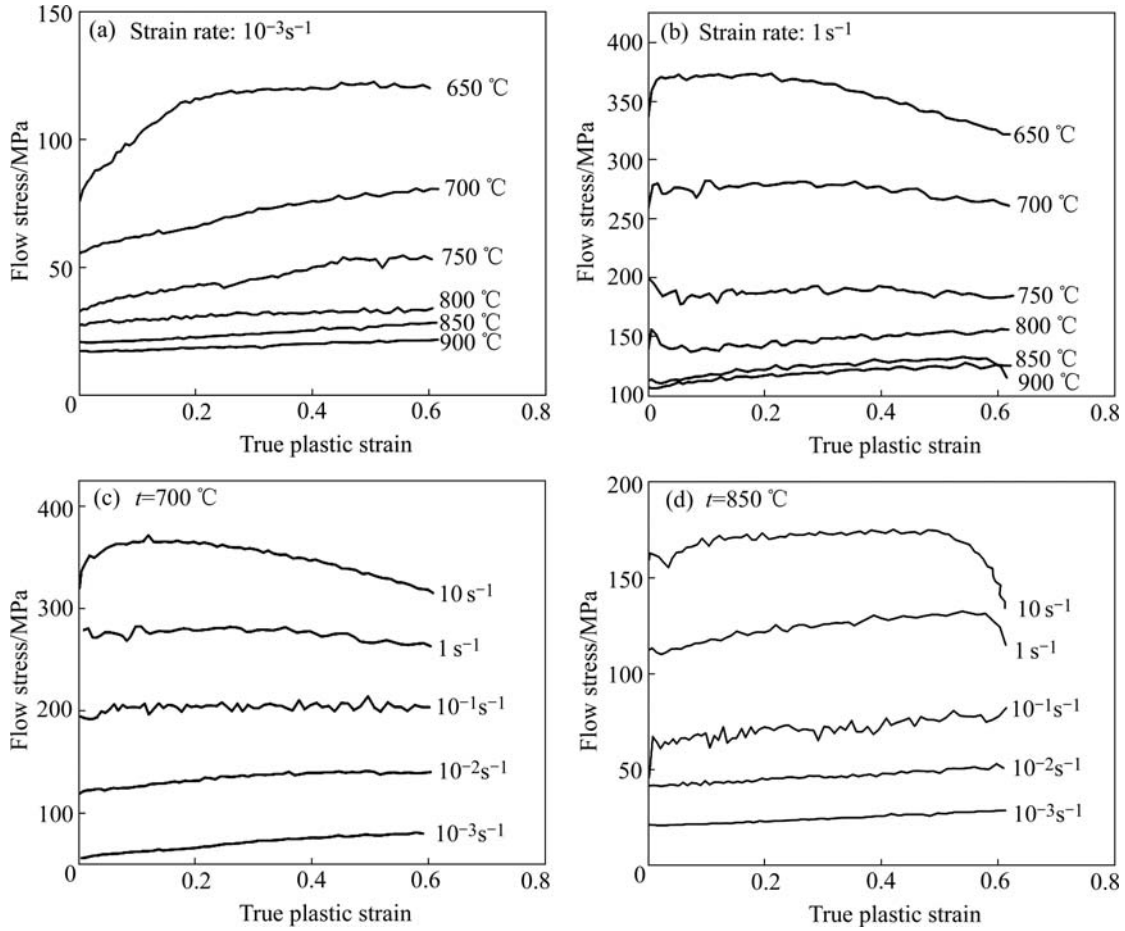

Fig.2 Curves of true strain vs true stress of Ti-1023 alloy in compression test under different conditions

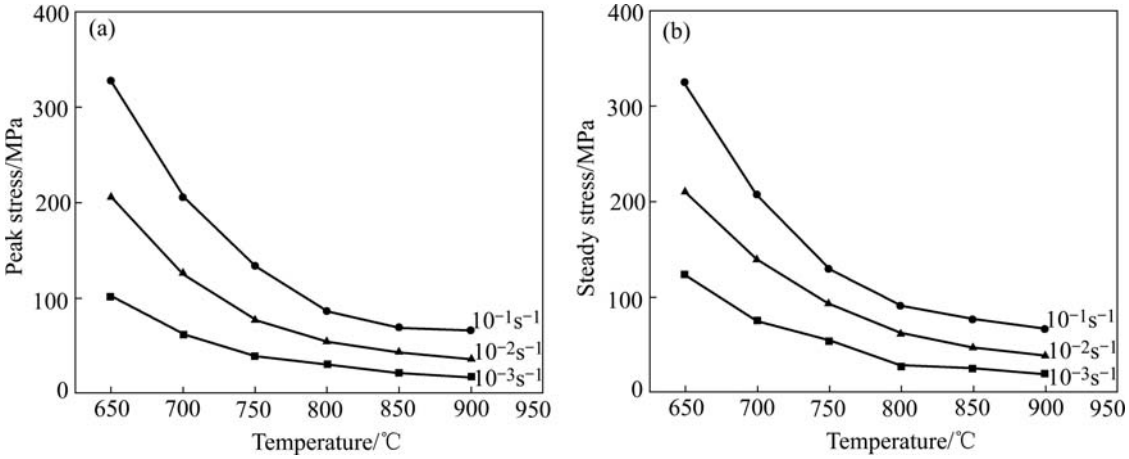

Fig.3 Relationships among peak stress(a) steady stress(b) and temperature

the data in Fig.4 exhibit a curve, suggesting that its slope is strain rate dependent. For an approximation, the strain rate dependence may be split into two regimes: one below the strain rate of 0.1 s^{-1} and the other at higher strain rates. The values of n from two slopes are estimated to be 4.4 and 6.7, respectively. In a limited strain rate range of 0.001−0.1 s^{-1} the kinetic rate equation is obeyed, and a linear fit is obtained at the temperatures.

In the α-β region(temperature lower than 802 ℃), the Arrhenius plot for estimating the apparent activation energy for hot deformation in the two phase region is shown in Fig.5(a). The plot shows that very good correlation exists at lower strain rates. It is pertinent to apply the kinetic rate equation (Eqn.(1)) in this range of temperature and strain rate. From such an analysis, it is estimated that the apparent activation energy is 322 kJ/mol. This is close to that reported by ROBERSTON

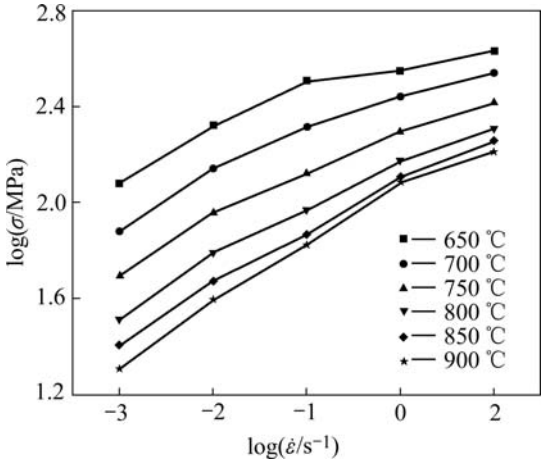

Fig.4 Relationship between steady flow stress and strain rate

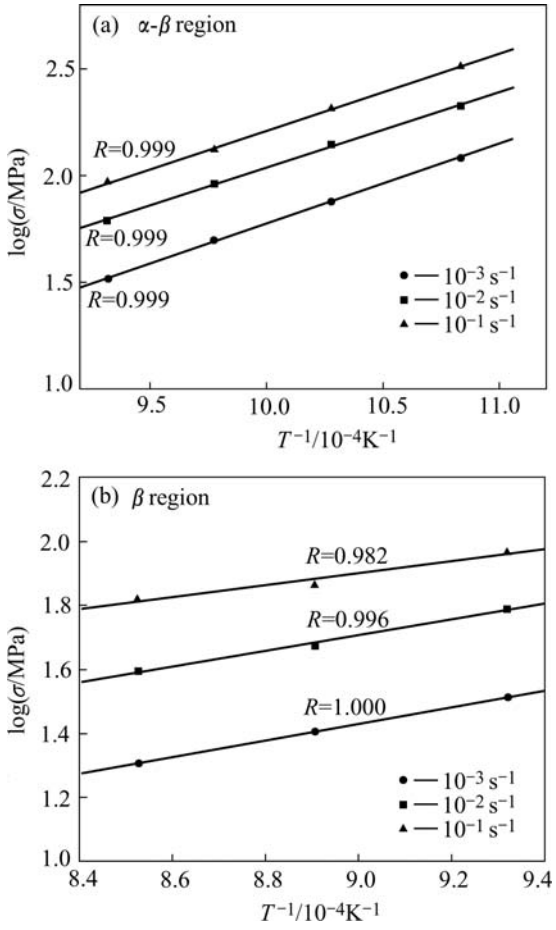

Fig.5 Variation of flow stress with inverse of temperature at different strain rates

and MCSHANE[12] (295 kJ/mol), and higher than that for self-diffusion in β-Ti (153 kJ/mol), for self-diffusion in α-Ti (169 kJ/mol) or diffusion of vanadium in β titanium(135 kJ/mol). This indicates that the dynamic recovery of β phase takes place in this domain. As for α phase, except for dynamic recovery, dynamic recrystalliztion will take place under appropriate condition. But the microstructure shows no dynamic recrystallization, so only dynamic recovery occurs in both α phase and β phase[12]. Continuing the analysis on the basis of the kinetic rate equation, the temperature compensated strain rate parameter, Z is given by:

$$Z=\dot{\varepsilon}\exp(Q/RT) \quad (2)$$

Parameter Z is evaluated on the basis of the above apparent activation energy and plotted as a function of flow stress in Fig.6. The plot exhibits a good fit for the data and confirms that the kinetic rate equation is obeyed in the limited temperature and strain rate range being considered.

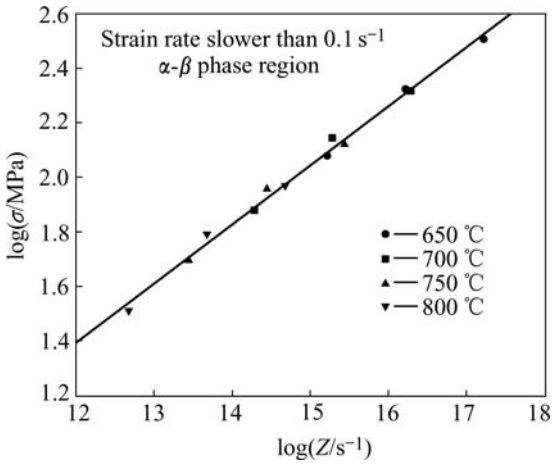

Fig.6 Variation of flow stress with Zener−Hollomon parameter (Z) of Ti-1023 alloy

In the β region, the Arrhenius plot is shown in Fig.5(b). The data fit at lower strain rates ($<0.1\ s^{-1}$) is very good. The apparent activation energy estimated from this plot is about 160 kJ/mol which is close to that for self-diffusion in β-Ti (153 kJ/mol). The value of apparent activation energy (185 kJ/mol) estimated by ROBERSTON and MCSHANE[12] is in agreement with the above values. The possible mechanisms in this domain are the dynamic recovery, dynamic recrystallization or superplastic deformation. Further analysis will discuss the microstructural characteristics of the process in this region later.

3.3 Processing maps

3.3.1 Power dissipation map

Processing maps of Ti-1023 alloy in this paper were developed through the method suggested by PRASASAD[9]. It is not only the cubic spline interpolation but the combination of the cubic spline interpolation and the polynomial fit that was used to develop the processing maps due to the numeric reliability of only the cubic spline interpolation[13]. The power dissipation maps obtained at strains of 0.4 and 0.6 are shown in Fig.7. The map in Fig.7(a) exhibits three

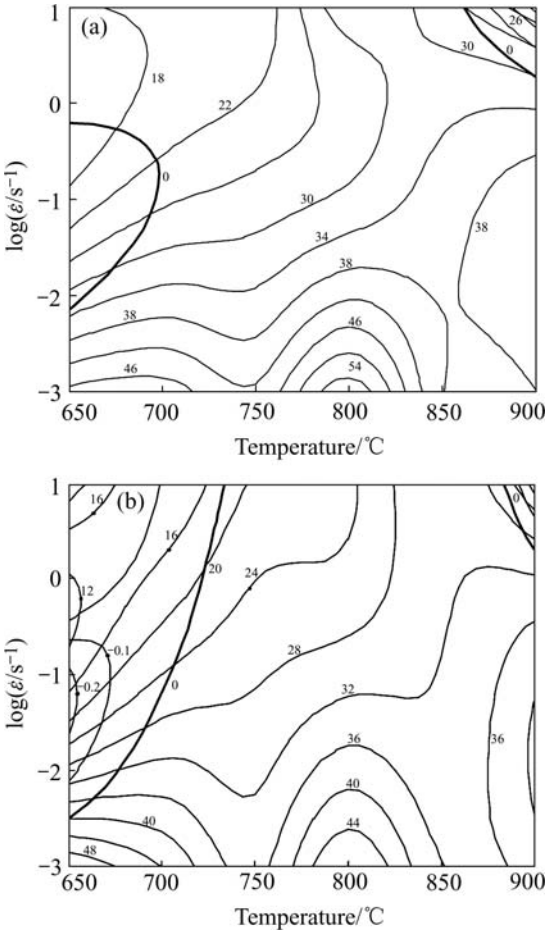

Fig.7 Processing maps of Ti-1023 alloy obtained at strain 0.4(a) and 0.6(b): numbers against contours represent efficiency of power dissipation expressed as percentage value; thick lines represent boundaries of instability regimes

domains—one in α-β temperature range, one near β transus and the other in β field. The domain in α-β temperature range occurs in the temperature range of 650−700 ℃ and at strain rate below about 0.03 s^{-1} with a peak efficiency of 47% at about 680 ℃ and 0.001 s^{-1}. The strain rate sensitivity of flow stress corresponding to the peak efficiency is about 0.32, which is close to that expected for superplastic deformation (0.5). The domain appears to extend to lower strain rate and may reach even higher peak efficiency value. The domain near β transus is in the temperature range 750−850 ℃ and strain rate range 0.001−0.03 s^{-1} with a peak efficiency of 56% at about 800 ℃ and 0.001 s^{-1}. The domain also appears to extend to lower strain rate and may reach even higher peak efficiency value. The power dissipation map shows the domain in the temperature range of 850−900 ℃ and strain rate range of 0.001−1 s^{-1} with the peak efficiency taking place at about 900 ℃ and 0.03 s^{-1}. With the increase of strain, the power dissipation map shows no obvious difference as the shown in Fig.7(b), except for the extension of the domain in β field.

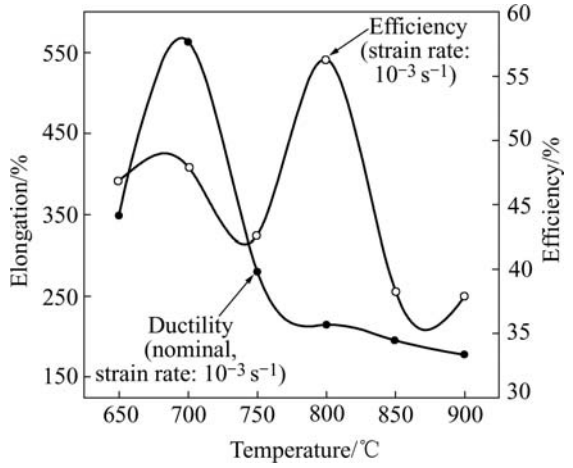

Fig.8 Variation of tensile ductility and efficiency of power dissipation with temperature for Ti-1023 alloy at normal strain rate 0.001s^{-1}

The tensile elongation(Fig.8) was measured as a function of temperature at a normal strain rate close to 0.001 s^{-1}. The elongations below β transus are abnormally high and confirm the occurrence of superplastic deformation. A peak value of elongation 564% occurs at 700 ℃, which is close to the temperature at which the local maximum in efficiency occurs in this domain. The microstructure of the specimens deformed at 650, 700 and 750 ℃ at strain rate of 0.001 s^{-1} or 0.1 s^{-1} are shown in Fig.9. It can be seen that α phase volume fraction decreases with increasing temperature. At strain rate of 0.001 s^{-1}, the microstructure deformed at 650 ℃ exhibits a lot of tortuous α phase, which is much longer than that deformed beyond 700 ℃. The less tortuous α phase and lower volume fraction are obtained at 700 ℃, and no tortuous α phase is observed at 750 ℃ due to shorter α phase. From the microstructures shown in Figs.9(b) and (c), it is found that α phase at higher strain rate (0.1 s^{-1}) is more tortuous than that at lower strain rate(0.001 s^{-1}). This indicates that at higher strain rate α phase is more easily broken up. The mechanism of superplastic deformation involves the sliding of grain (or phase) boundaries and accommodation, through plastic deformation and mass movement of directional diffusion, of the resulting stress concentration at the grain boundary triple junction. Mass movement of directional diffusion needs low strain rate and is not obvious above 0.001 s^{-1}. Therefore, plastic deformation and the sliding of grain boundary are the main mechanisms for superplastic deformation in this domain. In terms of the sliding, proper proportion of two phases will be desirable for greater superplasticity. By calculation, the volume fraction of two phases are equal at about 680 ℃, which is close to the peak elongation. This confirms that when the volume fractions of two phases are equal, high ductility would be obtained in α+β alloys[14], because

the proportion of two phases is conducive to the sliding of α phase (β phase as viscoplastic medium). However, at lower temperature(650 ℃) both the lower volume fraction of β phase and the longer α phase(Fig.10(a)) give rise to some difficulty to the sliding of two phases. Therefore the plastic deformation, as indicated by tortuous α phase, is required to accommodate the resultant stress, so lower tensile elongation is obtained. At higher temperature(750 ℃), the shorter α phase and the higher volume fraction of β phase(Fig.10(b)) are not conducive to the sliding of two phases, and thus the tensile elongation deceases.

In the domain near β transus, the tensile ductility is considerably high(215% at 800 ℃), although not as high as that at lower temperature. Since this domain occurs at temperature near β transus, the domain is related to the deformation behavior of the β phase. The microstructure(Fig.11) of the specimen deformed at 800 ℃ and 0.001 s^{-1} exhibits large grains(average grain size about 60 μm),within which a stable and fine subgrain structure has developed. Such a microstructure is typical of large grain superplasticity(LGSP), which has been reported for Ti-1023 alloy[15], Ti-6Al-4VELI[16] and other β alloys[17]. The mechanism of LGSP is not well understood, but is thought to consist of the sliding of subgrain boundaries and accommodation of the stress concentration at their triple junctions by diffusional flow[16].

A typical of microstructure(Fig.12) deformed in domain in β phase field shows dynamic recrystallization microstructure. Therefore, dynamic recrystallization occurs in this domain.

3.3.2 Instability map

Compared the instability map at strain of 0.4 with that at strains 0.6, it is found that instability regimes take place in high temperature or low temperature with high instability map at strain of 0.6 exhibits two instability regimes: one is in the temperature range of 650−725℃

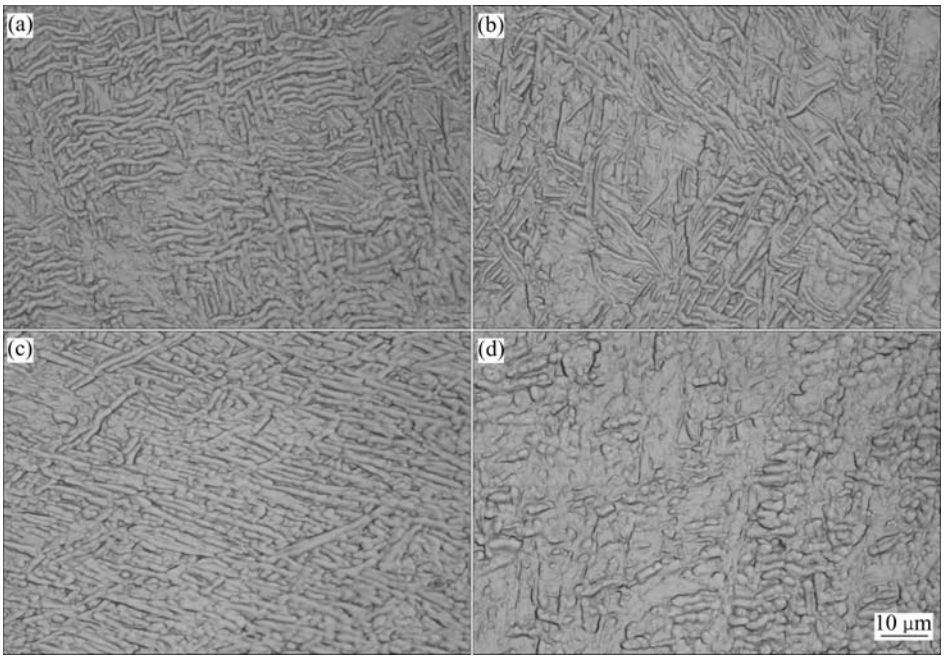

Fig.9 Optical microstructures of Ti-1023 alloy deformed at different temperatures and strain rates: (a) 650 ℃, 0.001 s^{-1}; (b) 700 ℃, 0.001 s^{-1}; (c) 700 ℃, 0.1 s^{-1}; (d) 750 ℃, 0.001 s^{-1}

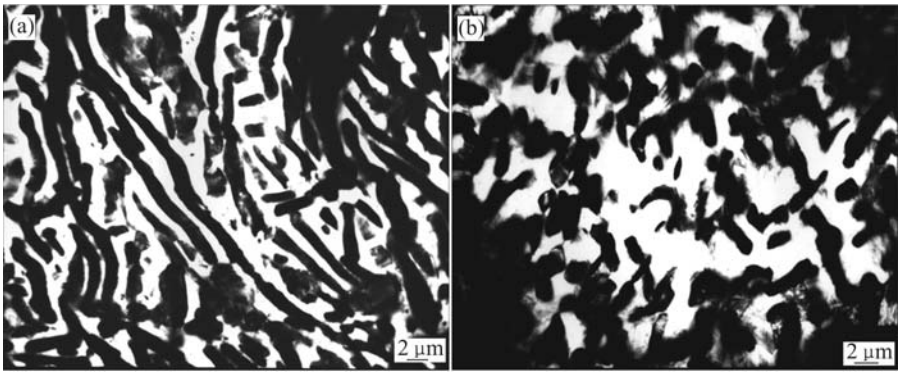

Fig.10 TEM photographs of Ti-1023 alloy: (a) 650 ℃, 0.001 s^{-1}; (b) 750℃, 0.001 s^{-1}

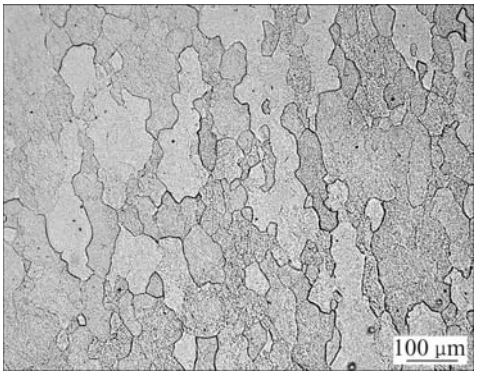

Fig.11 Microstructure of Ti-1023 alloy deformed at 800 ℃ and 0.001 s^{-1}

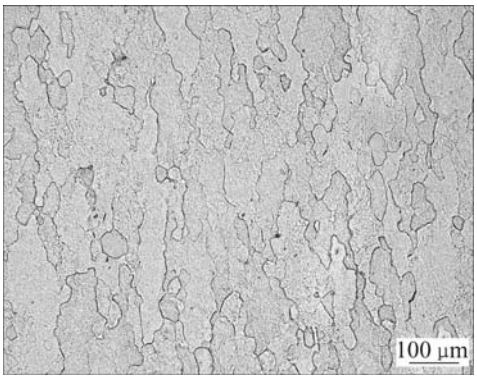

Fig.12 Microstructure of Ti-1023 alloy deformed at 900 ℃ and 0.01s^{-1}

and strain rate range of 0.01−10 s^{-1} which is validated by observing the microstructure shown in Fig.13, the other is near 900 ℃, 10 s^{-1}. In high temperature range, the microstructure will change due to phase transformation and so on during cooling to room temperature. Therefore, it is very difficult to validate by observing microstructure.

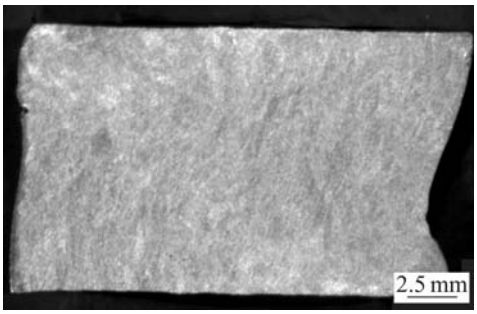

Fig.13 Macrostructure of Ti-1023 after deformation at 650 ℃ and 10 s^{-1}

4 Conclusions

1) In the temperature range of 650−750 ℃ and at strain rates below 0.03 s^{-1} with a peak efficiency of 47% at 680 ℃ and 0.001 s^{-1}, the material exhibit superplasticity marked by abnormal elongation with a peak at 700 ℃.

2) In the temperature range of 750−850 ℃ and strain rates range of 0.001−0.03 s^{-1} with peak efficiency at 800 ℃ and 0.001 s^{-1}, the large grain superplasticity takes place. Dynamic recrystallization occurs in the temperature range of 850−900 ℃ and strain rate range of 0.001−1 s^{-1}.

3) The instability map of this alloy exhibits two instability regimes: one is in the range of 650−725 ℃/ 0.01−10 s^{-1}, the other is near 900 ℃, 10 s^{-1}.

References

[1] WEISS I, SEMIATIN S L. Thermamechanical processing of beta titanium alloys- an overview[J]. Mater Sci Eng A, 1998, A243: 46-65.

[2] FROES F H, BOMBERGER H B. The beta titanium alloys[J]. JOM, 1985(7): 28-37.

[3] MAEDA T, OKADA M. Improvement of strength and fracture toughness in isothermally forged Ti-10V-2Fe-3Al[A]. Titanium '95: Science and Technology(Vol. Ⅱ)[C]. Birmingham, 1996. 948-955.

[4] DUERIG T W, TERLINDE T G, WILLIAMS J C. Phase transformation and tensile properties of Ti-10V-2Fe-3Al[J]. Metall Trans A, 1980, A11(12): 1987-1998.

[5] TERLINDE T G, DUERIG T W, WILLIAMS J C. Microstructure, tensile deformation, fracture in aged Ti-10V-2Fe-3Al[J]. Metall Trans A, 1983, A14(10): 2101-2115.

[6] BOYER R R, KUHLMAN G W. Processing properties relationship of Ti-10V-2Fe-3Al[J]. Metall Trans A, 1987, A18(12): 2095-2103.

[7] ROBERSTON D G, MCSHANE H B. Isothermal hot deformation behavior of metastable β titanium alloy Ti-10V-2Fe-3Al[J]. Mater Sci Technol, 1997, 13(7): 575-583.

[8] PRASAD Y V R K, GEGEL H L, DORAIVELU S M, MALAS J C, MORGAN J T, LARK K A, BARKER D R. Modeling of dynamic material behavior in hot deformation: forging of Ti-6242[J]. Metall Trans A, 1984, A15(10): 1883-1892.

[9] PRASAD Y V R K, SESHACHARYULU T. Hot deformation modeling for microstructureal control[J]. Inter Mater Rev, 1998, 43: 243-258.

[10] PRASAD Y V R K, SESHACHARYULU T, MEDEIORS S C, FRAZIER W G. Effect of prior β-grain size on the hot deformation behavior of Ti-6Al-4V: Coarse vs coarser[J]. J Mater Eng Perf, 2000, 9(2): 153-160.

[11] PRASAD Y V R K, SESHACHARYULU T. Processing maps for hot working of titanium alloys[J]. Mater Sci Eng A, 1998, A243: 82-88.

[12] ROBERSTON D G, MCCSHANE H B. Analysis of high temperature flow stress of titanium alloy IMI550 and Ti-10V-2Fe-3Al during isothermal forging[J]. Mater Sci Technol, 1998, 14(2): 339-345.

[13] BOZZINI B, CERRI E. Short communication numerical reliability of hot working processing maps[J]. Mater Sci Eng A, 2002, A328: 344−347.

[14] SEMIATIN S L, SEETHARAMAN V, WEISS I. The thermamechanical processing of alpha/beta titanium alloys[J]. JOM, 1997(7): 33-68.

[15] MORGAN G C, HAMMOND C. Superplastic deformation properties of β-Ti alloys[J]. Mater Sci Eng, 1987,86:159-177.

[16] PRASAD Y V R K, SESHACHARYULU T, MEDEIORS S C, FRAZIER W G. Effect of preform microstructure on the hot working mechanisms in ELI grade Ti-6Al-4V: transformed β v. equiaxed(α+β)[J]. Mater Sci Technol, 2000, 16: 511-516.

[17] GRIFFITHS P, HAMMOND C. Superplasticity in large grained materials[J]. Acta Metall, 1972, 20: 935-945.

(Edited by LONG Huai-zhong)